We recorded an increase in the number of spikelets and flowers, compatible with the branch increase. However, a larger fraction of mutants' flowers was sterile, with caryopses aborted or not formed at all, reaching the maximum value in the Volano *FT-L1*^{T145I} line. This sterility causes no change in the grain yield but supports the hypothesis of *FT-L1* being necessary for specifying floral identity.

In conclusion we demonstrated that flowering time in rice depends on a regulatory module, comprising not only *Hd3a* and *RFT1* but also *FT-L1*. FT-L1 is strongly induced during floral commitment and the florigens themselves and regulates the VM-to-IM conversion. It also promotes meristem reproductive development from IM to further reproductive stages, down to floret determinacy.

4.3.1 A common mechanism for inflorescence determinacy among grasses

We propose that this module is not limited to rice and panicle-type inflorescences, but rather a shared mechanism within grasses, including those producing spike-type inflorescences.
This hypothesis is corroborated by the role performed by orthologues of *OsFT-L1* in other temperate cereals.

The closest homolog genes to *OsFT-L1* in *Brachypodium distachyon* (*Bd*), barley (*Hordeum vulgare L., Hv*) and tetraploid wheat (*Triticum turgidum* ssp. *durum, Td*) are, respectively, Bd*FT2*, *HvFT2* and *FT-A2/FT-B2* (fig.47) [101].

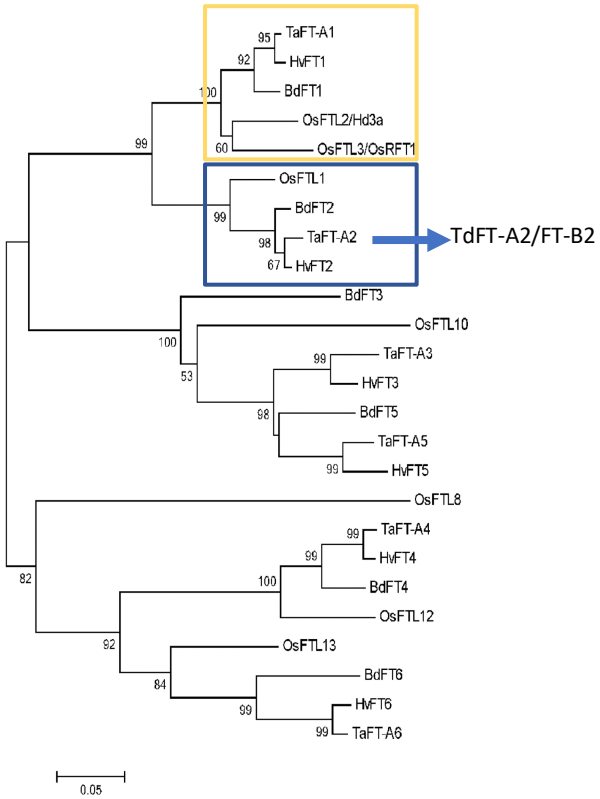

Figure 47 - Phylogenetic analysis of FT-like genes in temperate grasses. *The phylogenetic analysis was performed using a neighbor-joining tree constructed with the program MEGA 5.0 using the full-length proteins. The scale bar 0.05 represents 5% base substitution. Bootstrap numbers larger than 50 are shown in the respective nodes.*
The yellow box includes genes encoding for the florigens involved in the flower commitment; the blue box includes FT-L1-like genes. In this blue clade I added the A- and B- homeologs of Triticum turgidum ssp. Which are orthologues of TaFT-A2. This figure is adapted from [101].

In **barley**, *HvFT2* is expressed specifically in the inflorescence meristem and its expression increases during spike development as for rice *OsFT-L1*[102].

Furthermore, heading date and spike architecture were evaluated in *HvFT2* RNAi lines, to assess if there were any phenotypical differences compared to the controls. Transgenic $FT2_{RNAi}$ plants headed 4 days later with a reduction of 20.6% in fertility consisting in a decreased number of grains per spike (fig.48A,B), resembling Volano *FT-L1* mutant plants grown in the field [102].

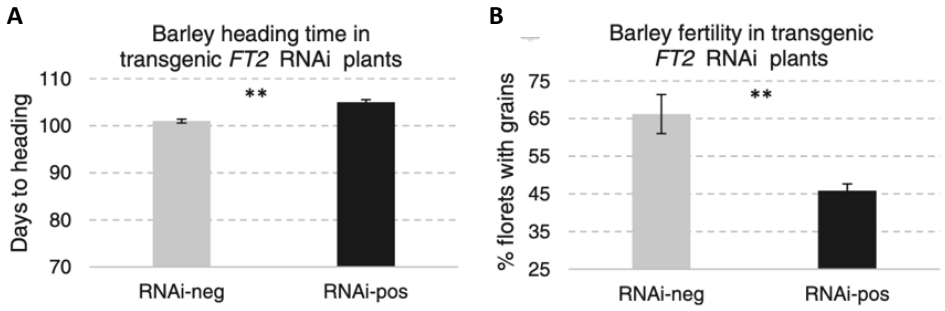

Figure 48 – Barley $FT2_{RNAi}$ transgenic plants. *A. Average heading time of barley FT2RNAi-positive plants and FT2RNAi-negative control plants. B. Average percentage of florets with grains in FT2RNAi-positive and FT2RNAi-negative plants* [102].

Overexpression of *BdFT2* under maize constitutive promoter caused a very early flowering phenotype with plants carrying less spikelets per spike [102]. These results are comparable to those obtained by overexpressing *FT-L1* (my work and Izawa[18]).

Moreover, a similar effect has been reported in **Brachypodium**, where overexpression of *BdFT2* in calli caused early heading date while still in the regeneration medium. Spikes of these shoots were shorter with few spikelets and no seeds. The opposite phenotype was obtained for $BdFT2_{RNAi}$: a flowering delay of about 8 days was recorded in down-regulated plants, showing a 25.9% reduction in fertility (fig.49A,B)[102].

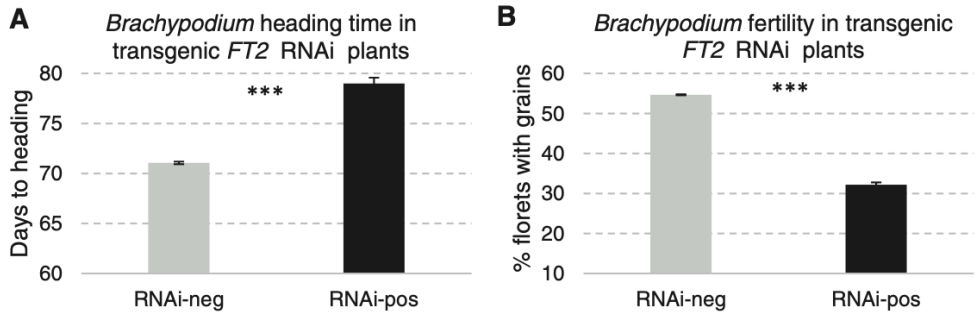

Figure 49 – Brachypodium distachyon $FT2_{RNAi}$ transgenic plants. *A. Average heading time of B. distachyon FT2RNAi-positive plants and FT2RNAi-negative control plants. B. Average percentage of florets with grains in FT2RNAi-positive and FT2RNAi-negative plants* [102].

For what concerns **tetraploid** wheat, two mutated lines were selected for *FT-A2* and for *FT-B2*, and both were analyzed for heading. While for *ft-B2* no significant delay was shown, for *ft-A2*, a small but significant delay of 2-4 days was detected. These evidences underline that *FT2* has a limited role in the transition from vegetative to reproductive meristem, differently from Brachypodium *BdFT*, from barley *FT2* and from rice *OsFT-L1*.

However, in *ft2-null mutants* spikelet number was strongly affected: *ft-B2* mutants differentiated more spikelets than the wild type and in plants carrying *ft-A2* and *ft-B2* an increase was detected in the number of spikelets per spike and florets per spikelet, as well as a reduction of fertility. This phenotype suggests a specific role for these genes in spike development and determination [102].

Furthermore, transcript levels of *FT2* were detected increasing quickly between the lemma primordium and terminal spikelet stages, reaching the peak at the W3.5 stage of Waddington scale, where floret primordium is present (fig.50A,B)[102,103]. This peculiar expression pattern differentiates this gene from *FT1* which is expressed in the leaf and shares the function with *Hd3a* and *RFT1* as key activator of flowering[103]. At the same time, *FT2* expression pattern is very close to the one of *OsFT-L1* and *HvFT2* which were observed in meristem tissues, corroborating the idea that genes of this clade function in the switch between IM to SM development. Furthermore, *FT-A2* and *FT-B2* expressions were higher in the distal part of the early developing spike, where new lateral spikelets and terminal spikelets are formed. This suggests the possibility that their involvement in the time-regulated formation of the terminal spikelet is crucial for the final determination of the total number of spikelets per spike.

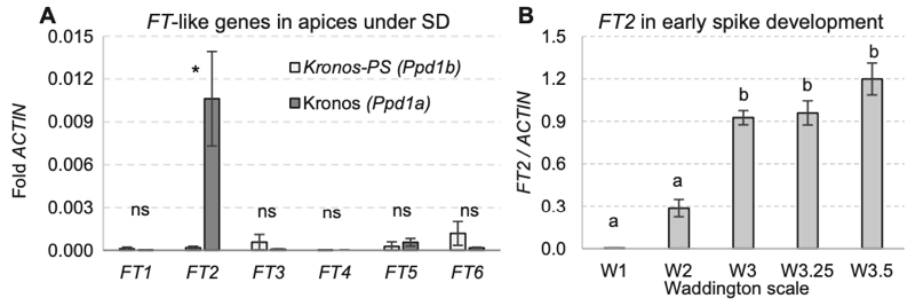

Figure 50 – Wheat FT-like transcript levels in apices and developing spikes.
A. Expression levels of FT-like genes in apical meristems of Kronos variety photoperiod-sensitive (with Ppd1b allele) and photoperiod-insensitive (with Ppd1a allele). B. FT2 transcript levels during early spike development. Waddington scale: W1, vegetative stage; W2, double ridge stage; W3, glume primordium present; W3.25, lemma primordium present; W3.5, floret primordium present [102].

Hence, the reduced florets fertility in wheat, barley and *B. distachyon ft2* or $FT2_{RNAi}$ mutant plants underlies a conserved role for *FT2* genes across grasses, corroborated by the phenotype of reduction in florets fertility observed in Volano *FT-L1* mutant plants.

This evidence suggests a conserved function of *FT2* genes among several species. The phylogenetic tree of fig.47 [101] shows a different clusterization of two families of florigens: those related to Hd3a and RFT1, and those more similar to FT-L1. The two clusters are also associated to different functions. While genes in the former group are involved in reproductive commitment by promoting the transition from VM to IM (see yellow box), the latter are involved in additional stages of inflorescence development (see blue box). In this last clade, indeed, all the genes included together with *OsFTL1*, are involved in the differentiation and determination of the SM and in floret fertility, suggesting a common origin of the function within Poaceae.

4.4 EMS *rft1* VOLANO MUTANTS AFFECT FLOWERING TIME, PANICLE BRANCHING AND FERTILITY

During my PhD, in addition to focusing on FT-L1 as a main project, I also dealt with the characterization of two mutants in another protein, the florigen RFT1.

These mutants were obtained through the same EMS chemical mutagenesis procedure, isolated from the mutagenized population and then screened with the KeyPoint™ technology.

The mutants obtained and considered were two: RFT1^{S47F} and RFT1^{R174K} (fig.51A,B).

A

```
>RFT1 wt
MAGSGRDDPLVVGRIVGDVLDPFVRITNLSVSYGARIVSNGCELKPSMVTQQPRVVVGGNDMRTFY
TLVMVDPDAPSPSNPNLREYLHWLVTDIPGTTGATFGQEVMCYESPRPTMGIHRLVFVLFQQLGRQ
TVYAPGWRQNFSTRNFAELYNLGSPVATVYFNCQREAGSGGRRVYP

>RFT1 S47F
MAGSGRDDPLVVGRIVGDVLDPFVRITNLSVSYGARIVSNGCELKPFMVTQQPRVVVGGNDMRTFY
TLVMVDPDAPSPSNPNLREYLHWLVTDIPGTTGATFGQEVMCYESPRPTMGIHRLVFVLFQQLGRQ
TVYAPGWRQNFSTRNFAELYNLGSPVATVYFNCQREAGSGGRRVYP

>RFT1 R174K
MAGSGRDDPLVVGRIVGDVLDPFVRITNLSVSYGARIVSNGCELKPFMVTQQPRVVVGGNDMRTFY
TLVMVDPDAPSPSNPNLREYLHWLVTDIPGTTGATFGQEVMCYESPRPTMGIHRLVFVLFQQLGRQ
TVYAPGWRQNFSTRNFAELYNLGSPVATVYFNCQREAGSGGKRVYP
```

B

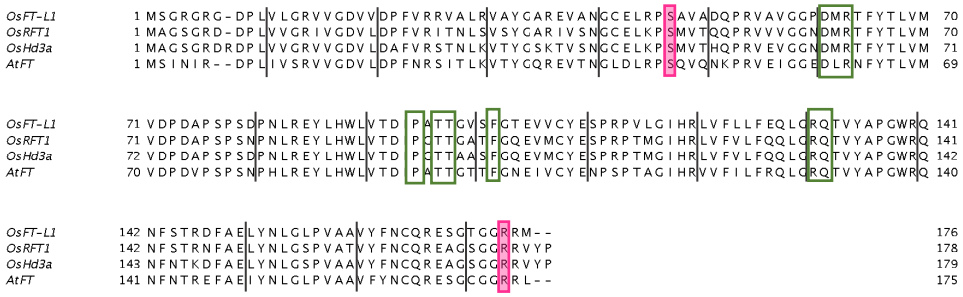

Figure 51 – Presentation of RFT1 EMS mutants. *A. Alignment of RFT1 WT and RFT1^{S47F} and RFT1^{R174K}. Residues substituted are in red, while the corresponding residues in the WT are in green. B. Alignment of FT-L1 with RFT1, Hd3a and Arabidopsis thaliana FT. Green boxes highlight the conserved amino acidic residues involved in binding with Gf14 proteins. The two conserved amino acids in pink boxes are those mutated in the RFT1 Volano lines.*

As it can be seen in the alignment of fig. 51B, the first mutant RFT1^{S47F} presents an amino acid substitution of a Serine in position 47 with a Phenylalanine. The second mutant RFT1^{R174K}, instead, presents a substitution of an Arginine with a Lysine, in position 174. Both these amino acids substitutions fall in residues entirely conserved in Hd3a, RFT1, OsFT-L1 and FT.

For these lines different phenotypes were evaluated. We first checked flowering time in both short day and long day conditions. Also in this case, since the mutations were obtained through chemical mutagenesis and not transgenesis, the analyses in long day were carried out in the field, thus being a natural long day (N-LD).

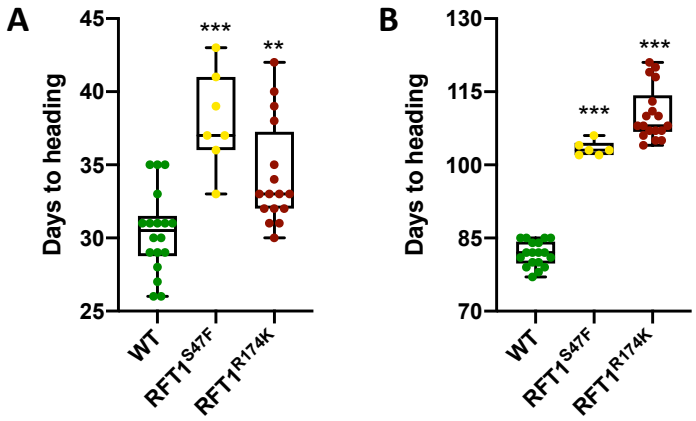

Figure 52 - Flowering time of RFT1 Volano mutants under SD (A) and natural LD in the field (B).
*Flowering time under SD conditions has been measured in greenhouses while flowering time under NATURAL LD has been measured in a Vercelli field. Each dot represents one plant and is color-coded depending on the genotype. ** P<0.01 and *** P<0.001, p values are obtained by unpaired two-tailed Student's t-test with Welch correction, measured relative to the WT.*

As can it be seen in the first graph (fig.52A), in SD conditions both lines show a statistically significant delay in flowering, with a greater increase in days' number, in particular for RFT1^{S47F} line. Same phenotype of delayed flowering was observed under N-LD conditions (fig.52B), for both lines showing a strong delay compared with WT. It can therefore be concluded that both these amino acid substitutions lead to a strong delay in flowering time.

To assess if there was any phenotype on the panicle architecture, we examined panicles through the P-TRAP software[100], with which we analyzed various traits, including the number of branches. To perform this analysis, we used panicles from the same plants scored for heading date.
As anticipated the analysis was carried out on all traits but the most interesting data concern the ramifications, both primary and secondary.

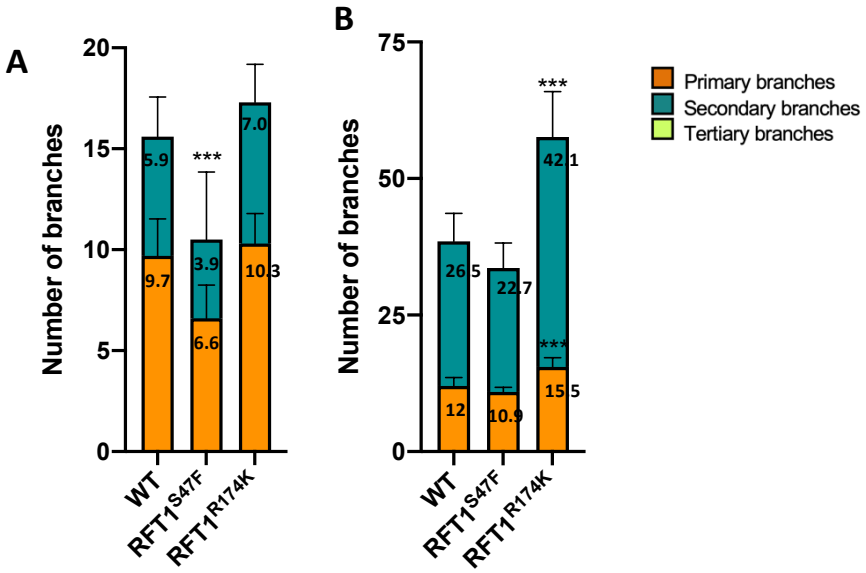

Figure 53- Quantification of panicle branching in Volano mutants under SD (A) and natural LD in the field (B). *Data were obtained with the P-TRAP software[100] and indicate the mean ± standard deviation of ten panicles per genotype collected from the main culms (means are reported on the histograms). *** P<0.001 are based on unpaired two-tailed Student's t-test with Welch correction.*

Regarding panicles grown under inductive SD conditions (fig.53A), the number of branches didn't show significant increase in any line. It was therefore possible to genetically separate the two phenotypes and we concluded that increased panicle branching is not correlated to delayed flowering, thus providing a corroboration of how one phenotype is not a consequence of the other. As previously described, indeed, a delay in vegetative-to-reproductive transition could lead to panicles with more branches. However, in the case of mutations in RFT1, this correlation was not observed.

Regarding the analysis in LD conditions (fig.53B), we observed a strong increase in the number of both primary and secondary branches for the RFT1^{R174K} line. Interestingly, these data suggest that in the BM determination this florigen, too, plays a crucial role. Differently from FT-L1, in RFT1 panicles there is an increase in the number of primary branches as well, thus highlighting a probable delay in branch identity determination.

Finally, it was of our interest to evaluate whether there was any effect in the late stages of development, in particular we considered fertility and for this trait, we counted the fertile and sterile flowers. For both lines there was a sharp increase in sterile flowers in comparison to WT plants (fig.54).

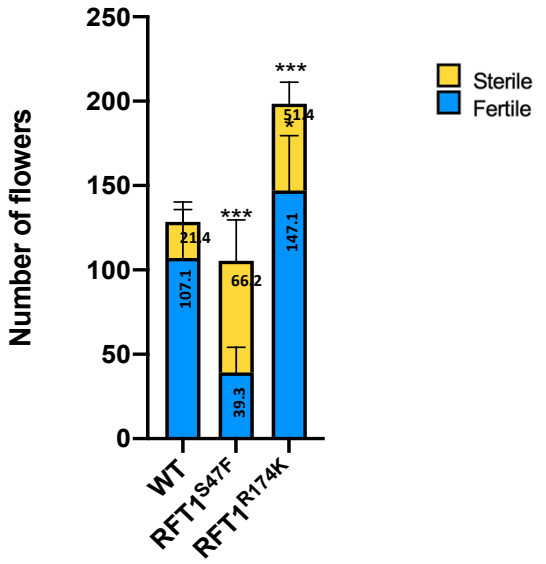

Figure 54 - Quantification of panicle fertility in RFT1 Volano mutants*. Data indicate the mean ± standard deviation of sterile and fertile flowers collected from the ten panicles analyzed with the P-TRAP software. The means are reported on the histograms. * P<0.05 and *** P<0.001 are based on unpaired two-tailed Student's t-test with Welch correction. Sterile flowers are those not giving rise to a caryopsis or those aborting it precociously.*

In particular, in RFT1^{R174K} line, that showed an increased number of primary and secondary branches there was an increase in the total number of flowers, mostly due to the larger fraction of fertile flowers; while in RFT1^{S47F} line, flowers' total number remained limited, consistently with the reduced branch number.

In fig.55A-C it is possible to notice the picture of Volano RFT1 EMS mutants' panicles.

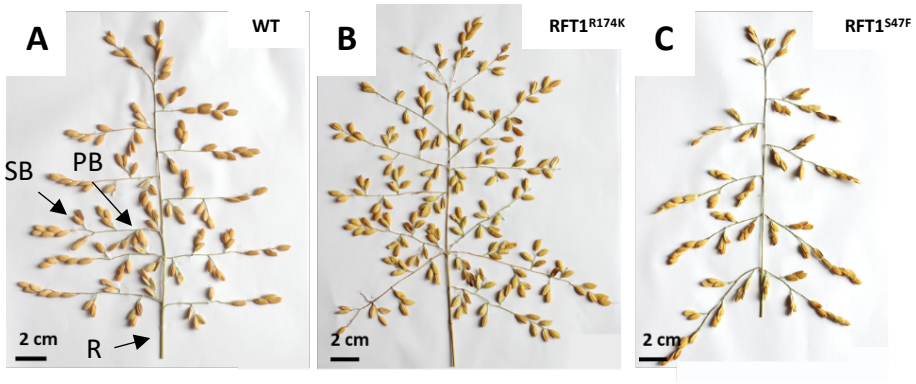

***Figure 55 - Representative pictures of panicles of the indicated genotypes**. A. Volano WT; B. Volano RFT1^{R174K}; C. Volano RFT1^{S47F}; R, Rachis; PB, Primary branch, SB, Secondary Branch. Scale bar, 2 cm.*

In conclusion, the data obtained suggest that also RFT1 has a role in stages following the commitment in particular in branch and spikelet meristems' determination.

Lastly, since RFT1 mutants also showed branching phenotype, in these months we are undertaking analysis to evaluate whether there is an additive effect between FT-L1 and RFT1 in the determination of the branches. We are in fact working on crossings of the lines that showed a notable increase in branching: homozygotes for the RFT1^{R174K} line crossed with homozygotes of the FT-L1^{P95S} line and the FT-L1^{G117R} line.
The seeds will be sown in fields in Tortona during the 2022 cropping season. Once the plants are ready, flowering time and panicle traits will be quantified, to understand whether the addictive effect on flowering (phenotype recorded in CRISPR lines) is conserved in Volano cultivar, and to evaluate if the additive effect concerns also the determination of the number of branches.
These analyses suggest an additional function of *RFT1* having the dual role of florigen responsible for the transition from VM to IM and from IM to PBM/SBM. At this point, it would be intriguing to understand if *Hd3a* could also act at later developmental phases, after the commitment, as for *FT-L1* and *RFT1,* and whether it does play a role in the development of the ramifications. To assess this last hypothesis further experiments must be performed.

4.5 FT-L1 ACTS DOWNSTREAM OF SPLS TO CONTROL PANICLE BRANCHING

The shift from VM to IM is the direct result of a synergic role of florigens, Hd3a and RFT1, together with FT-L1. But how FT-L1 could be transcriptionally regulated during subsequent developmental stages after the commitment remains unclear.
A ChIP-seq experiment performed by Lu et al. in 2013, showed that the *FT-L1* promotor is bound by SQUAMOSA PROMOTOR BINDING PROTEIN-LIKE 14/IDEAL PLANT ARCHITECTURE 1 (SPL14/IPA1, hereafter SPL14) about 2kb upstream of the transcription start site[72] *(see Introduction section 3.6)*.
Since SPL14-D gain-of-function plants show an increase in panicle branching, we have hypothesized that SPL14 could play the role of negative regulator of *FT-L1* transcription.

Our idea is summarized in this model:
Accumulation of *SPL* transcripts and protein implies that the *FT-L1* promotor is bound by the transcription

factor. This would cause a reduction in *FT-L1* expression which is no longer able to promote the SBM-to-SM switch causing an increase of branch number.

In order to validate this hypothesis, we first generated loss- and gain-of-function alleles of *SPL14* and then quantified *FT-L1* expression in these lines. To obtain them we used one single guide to edit both *SPL14* and *SPL17* at the same time. The rationale behind this approach is that *SPL14* and *SPL17* display an additive function[75]. They show a high sequence homology and share the same binding site for miRNA156. Furthermore, as previously mentioned, both are highly expressed in the young inflorescence[72]. The sgRNA was designed to target the miR156 binding site. Out-of-frame indels would produce loss-of-function *spl* mutants, while in-frame indels would produce gain-of-function *SPL-D.*

After transformation and selection of editing events we obtained the alleles and combinations listed in fig.56.

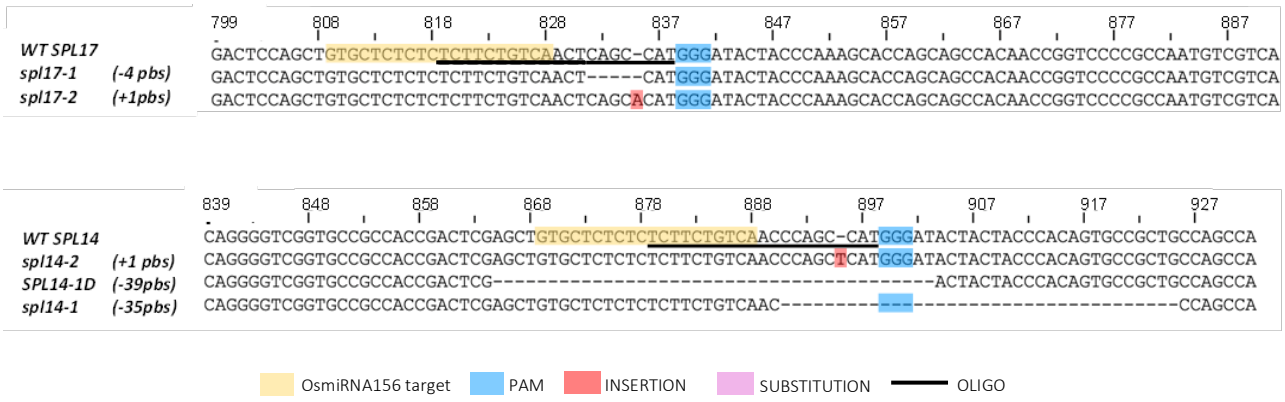

Figure 56 - Description of SPLs CRISPR mutants*. spl17 loss-of-function, spl14 loss-of-function and SPL14 gain-of-function (SPL14-1D) alleles are shown and aligned with MAFFT against the wild type. As shown in the legend, the position of the sgRNAs is underlined in the WT allele. The same sgRNA was used to target both SPLs simultaneously. In this experiment, we selected mutant lines homozygous for the spl17 loss-of-function alleles and harbouring either loss- or gain-of-function alleles for SPL14. Only the sequences around the sgRNA oligos location are shown.*

The combinations of alleles we selected for subsequent analyses, included *spl14-1 spl17-1* and *spl14-2 spl17-2* and *SPL14-1D/spl14-2 spl17-2*. The *spl14-1 spl17-1* and *spl14-2 spl17-2* have loss-of-function (l-o-f) alleles for both the *SPLs*, while the *SPL14-1D/spl14-2 spl17-2* has a biallelic mutation for *SPL14* – one allele is dominant gain-of-function (g-o-f) and the other one is loss-of-function– and loss-of-function alleles for *SPL17*. With these genotypes we could determine the effect of SPL14 on *FT-L1* expression in a common *spl17* mutant background.

To perform this experiment, we sampled the inflorescence at specific days after the shift to obtain panicles at secondary branch and floret stages. Yet, unexpectedly, *SPLs* mutants' panicles were not homogeneously developed, appearing too developed (for g-o-f lines) or too little (for l-o-f lines) and the developmental stages were very variable. These inconsistent phenotypes were probably due to a time-dependent developmental pattern, accelerated in g-o-f and delayed in l-o-f, that corroborates *SPLs* role in inflorescence activity promotion. Yet, it prevented proper measurement of *FT-L1* transcription. For the reasons described above, we sampled and organized biological replicates based on panicle morphology rather than counting the days

from the induction. In these lines we checked also *OsMADS15* expression as a marker of inflorescence development, to confirm that samples were homogeneous between and within genotypes (fig.57A).

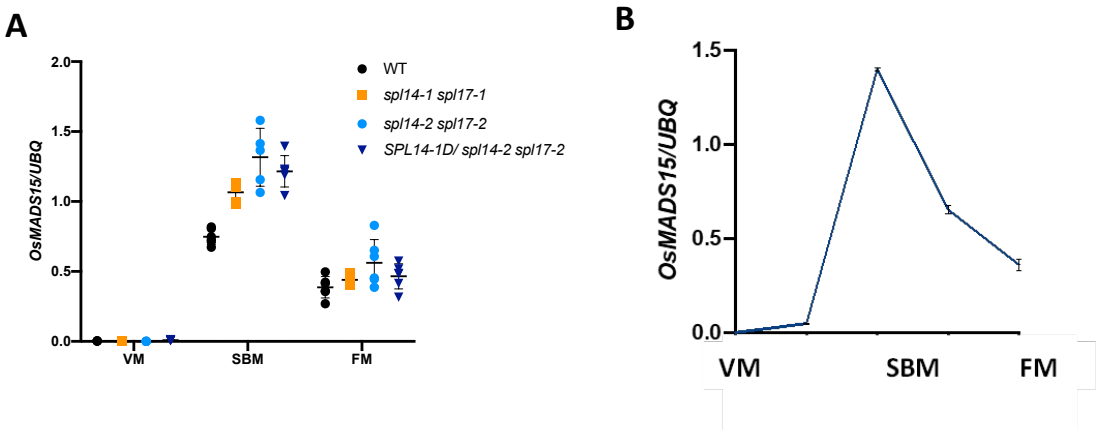

Figure 57 – Expression pattern of OsMADS15. *A. Quantification of OsMADS15 mRNA expression in the same genotypes as fig.56. Shoot apical meristems were collected at vegetative meristem (VM), secondary branch meristem (SBM) and floret meristem (FM) stages. The FM stage included flowers already developing floral organs. B. OsMADS15 expression trend during development. Each stage is represented by six points including two biological replicates, each of which including three technical replicates. Values were normalized on the housekeeper UBQ.*

We took advantage of its transcript quantification, well-known during all developmental stages, to create clusters of samples with the same expression levels. As visible in fig.57B, its expression follows a specific trend: no mRNA is detected at VM, then it is represented with a peak at PBM and SBM and again it decreases during the FM stage.

We then grouped samples at the same developmental stages (based on similar morphology and similar *OsMADS15* expression levels) and proceeded with real time quantification of *FT-L1* transcript (fig.58).

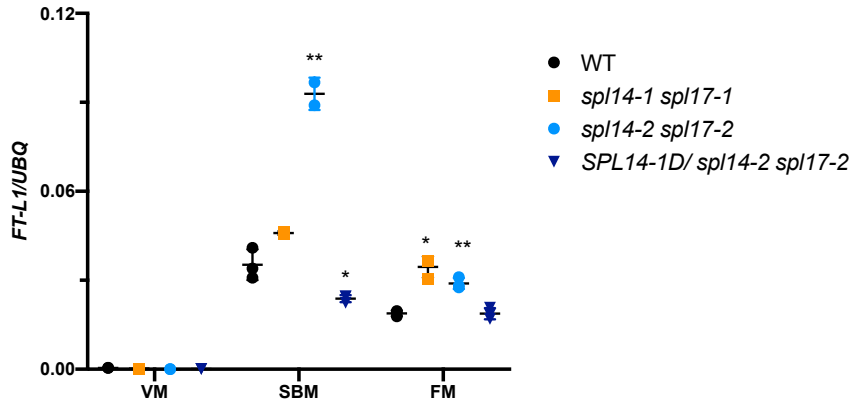

Figure 58 - Quantification of FT-L1 transcription in SPL loss and gain-of-function mutant backgrounds. *The genotypes were those of fig.55. VM, vegetative meristems; SBM, secondary branch meristems; FM, floral meristems. Each stage is represented by six points including two biological replicates, each of which including three technical replicates. * P<0.05 and ** P<0.01 are based on unpaired two-tailed Student's t-test with Welch correction.*

The results we observed, shown in fig.58, during the SBM stage showed that *FT-L1* expression increased in *spl14 spl17* double mutants, while it decreased when a *SPL14-D* dominant allele was in the background. At the FM stage when meristems are fully developed and determined, *FT-L1* transcription decreases both in mutants and in wt.

This evidence is consistent with our first hypothesis that *FT-L1* transcription is negatively regulated by *SPLs*. The data confirm that, during inflorescence development, when the branching pattern is elaborated, the *SPLs* contribute to repress *FT-L1* transcription to increase branch number, highlighting *FT-L1* function as an integrator of both the SPLs and photoperiodic pathways.
More interesting, at this point, is trying to speculate on how this function is performed since the relative expressions do not seem to overlap as *SPLs* are expressed in the bracts (fig.59A in pink, fig.59D) [5] while *FT-L1* in panicle branches (fig.59B in green, fig.59E).
However, one possible explanation is provided by Wang et al., by describing *SPLs* function, in regulating panicle branching, as non-cell autonomous factors[5].
Another option would be to reconsider the spatial expression domain of the SPLs. Indeed, looking at ISH published by Wang et al. (fig.59D), it could be noted that actually there is a residual signal of the *SPL* in the branches themselves (fig.59C, in pink), thus suggesting that *FT-L1*'s and *SPLs'* expression profiles do overlap, at least partially (fig.59C, in violet). In this second hypothesis, that residual expression, albeit little, could be enough to achieve the FT-L1 binding and repression. The construction of a fluorescent reporter for SPL14 would contribute to solve these issues.

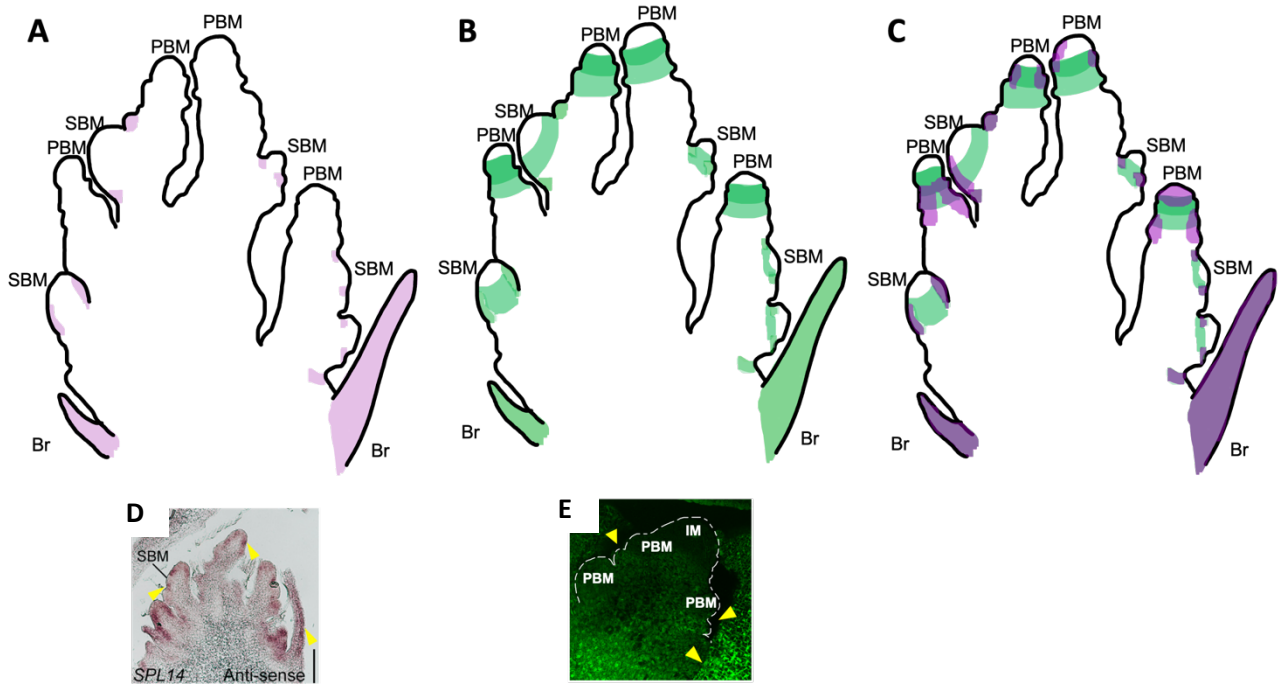

Figure 59 – Pattern of SPL14 expression at the Primary and Secondary Branch Stage *A. The sketch of SPL14 expression pattern (in pink) based on D., insitu hybridizations by Wang et al., 2021[5] at primary and secondary branch formation stage. The expression is localized in the bracts. B. The sketch of FT-L1 expression pattern (in green) based on E. our transcriptional marker lines shown before. The expression is both in the branches and bracts. For A. and B. yellow arrowheads point at bracts. C. The merge of the two sketches (A. and B.) representing SPLs and FT-L1 expression domains unveils an overlapping localization. For SPLs expression a more expanded profile was used, as described in the text. D. Insitu hybridization of SPL14 by Wang et al., 2021[5]. E. FT-L1 expression pattern in our pFT-L1:eYFP marker lines. Br, bracts; PBM, primary branch meristem; SBM, secondary branch meristem.*

4.6 FT-L1 OPERATES VIA FAC FORMATION

4.6.1 FT-L1 can interact with FAC components

To understand if FT-L1 interacts with the components of the F-A-Complex, whether or not it assembles FACs or if it assembles alternative ones, we decided to perform protein-protein interaction BiFC assays.
Since florigens interact with Gf14s we tested this interaction in particular with Gf14b and Gf14c, as representatives of the Gf14 family. We have previously shown that OsFD4 could interact directly with RFT1 but not with Hd3a[68], without the Gf14s as molecular bridges *(see Introduction section 3.5.2- Alternative FACs)*.
Therefore, also FT-L1 might be able to interact directly with OsFDs. We decided to test the interaction with OsFD1[60], OsFD4[68]and OsFD7[53] which are expressed in the meristem, as FT-L1.

The results of this analysis, with empty vectors, are shown in the panel of fig.60A-I.

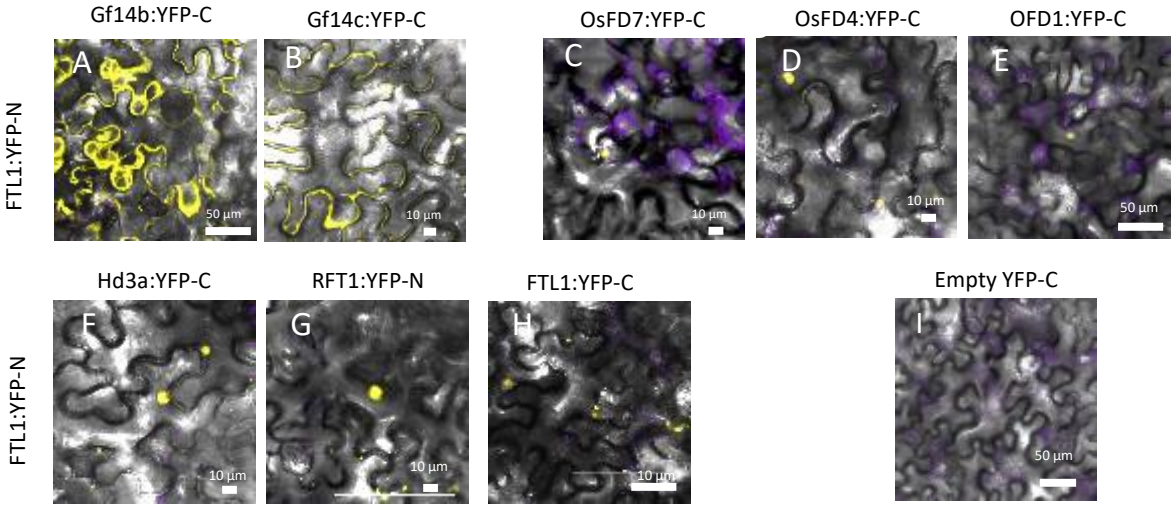

Figure 60 - Protein-protein interactions determined by BiFC of FT-L1 wt with Gf14s, OsFDs and florigens.
A. and B. represent the interactions with Gf14b and Gf14c respectively. C.-E. Show the interaction with the OsFDs as OsFD7, OsFD4 and OsFD1. F.-H show interactions with florigens as Hd3a, RFT1 and FT-L1 itself. FT-L1 has been cloned in pBAT TL-B sYFP-N vector (see Material and methods section). The reconstituted YFP is yellow while the chlorophyll is purple. Interactions with the Gf14s are localized in the cytoplasm, those with the OsFDs are localized in the nuclei, while those with the florigens are in nuclei. I. Negative control of BiFC protein-protein interaction assays using empty YFP-C vectors. This experiment was repeated three times with similar results. Additional pictures are shown in fig.64.

For this analysis we detected interactions between FT-L1 and the Gf14s (fig.60A,B), as visible by the yellow signal of the reconstituted YFP. The fluorophore is localized in cytoplasmatic subcellular compartment similarly to the well-known interactions of the florigens RFT1 and Hd3a with the Gf14s and validating the Taoka model of FT-GF14 that bind to each other in the cytoplasm of SAM cells before entering the nucleus and assembling the FAC with the last element FD[60].

For the interaction with the transcription factors OsFD1, OsFD4 and OsFD7 (fig.60C-E) we saw the reconstituted YFP in the nuclei within all OsFDs interaction tested, in particular we detected a very strong signal regarding the FT-L1-OsFD7.
For this last kind of results, the data are consistent with previous work [68] validating, in rice, the interaction florigen-bZIP than could also be direct, without the intercession of the Gf14s.

To complete the interaction assays with all FAC components, we also checked the interactions with the other florigens and with FT-L1 itself, to assess if it could homodimerize.

As shown in the panel (fig.60F-H), FT-L1 is able to interact directly with both florigens Hd3a and RFT1 and with FT-L1 in the nucleus subcellular compartment.
We don't know, yet, if the interaction with the florigens has a biological significance, further analysis must be run to corroborate it through in vivo analysis.

4.6.2 FT-L1^{P95S} can interact with FAC components

We decided to check also the interactions with FT-L1^{P95S} (fig.61A-H), one of the mutants obtained and previously described harboring the mutation in the P95 residue. As mentioned, this residue is one of those involved in binding with the Gf14s[60] (*see Results and Discussion section 4.2.2)*.

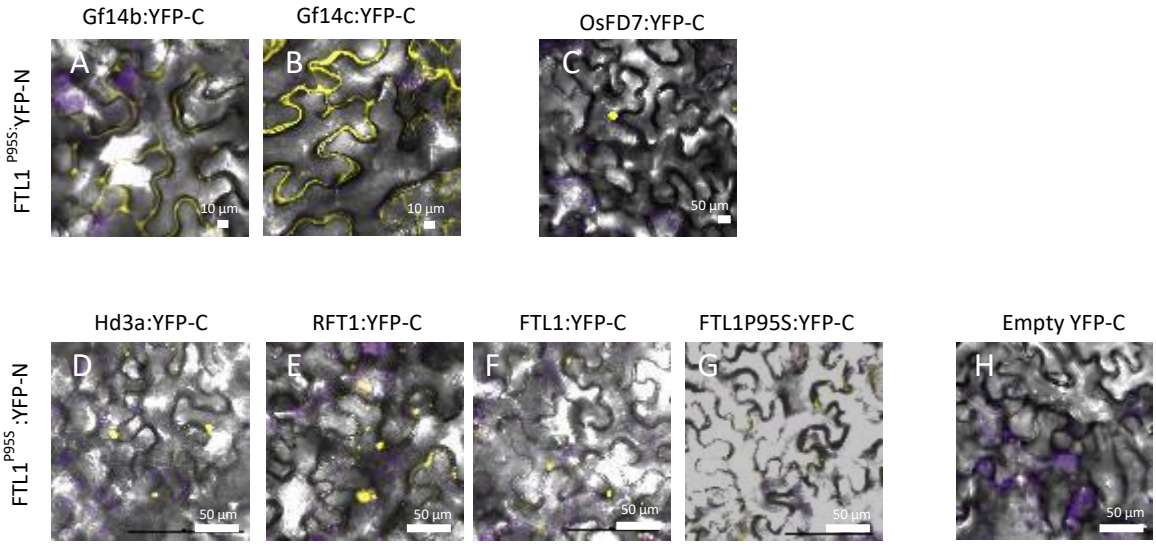

Figure 61 - Protein-protein interactions determined by BiFC of FT-L1^{P95S} with Gf14s, OsFD7 and florigens.
A. and B. represent the interactions with the Gf14b and Gf14c, C. is the interaction with OsFD7 while D.-G are the interactions with florigens as Hd3a, RFT1, FT-L1 both WT and P95S. FT-L1^{P95S} has been cloned in pBAT TL-B sYFP-N vector (see Material and methods section). The reconstituted YFP is yellow while the chlorophyll is purple. Interactions with the Gf14s are localized in the cytoplasm, those with the OsFDs are localized in the nuclei, while those with the florigens are in nuclei.
H. Negative control of BiFC protein-protein interaction assays using empty YFP-C vectors. This experiment was repeated three times with similar results. Additional pictures are shown in fig.64.

We hypothesized that the phenotypes observed in *FT-L1*^{P95S} plants could be due to failure to interact with Gf14s and assemble a FAC.

Unexpectedly, when tested the interaction with Gf14b and Gf14c (fig.61A,B), we detected the same cytoplasmatic reconstituted YFP, for both *FT-L1*^{P95S}–Gf14c and *FT-L1*^{P95S}–Gf14b, resembling results previously obtained for FT-L1 wt.

We next checked if FT-L1^{P95S} could interact with the OsFD7 as representative of OsFDs family (fig.61C). In FT-L1^{P95S}–OsFD7 interaction, the reconstituted nuclear signal was strongly detected.
For what concerns the interactions with florigens (fig.61D-G), FT-L1^{P95S} is once again able to interact directly with Hd3a and RFT1. It manages to heterodimerize with FT-L1 WT version (fig.61F) and homodimerize with itself (fig.61G).
All the signals were detected in the nucleus subcellular compartment as for the FT-L1 WT.

4.6.3 Quantification of interaction via FLIM-FRET

To further validate and quantify the interactions, we performed a FLIM assay on a selected group of proteins, including FT-L1 WT and FT-L1^{P95S} with Gf14s and OsFD7.

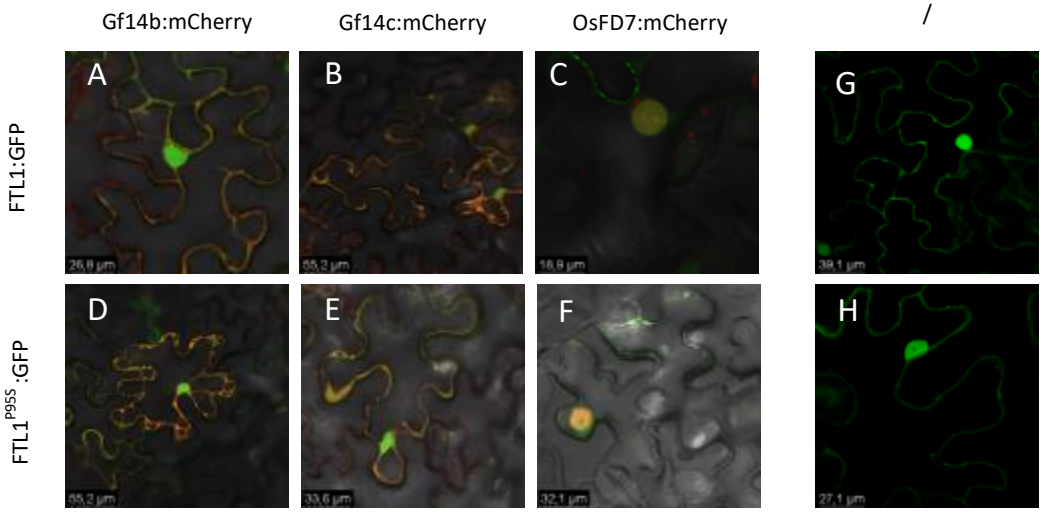

Figure 62 - Co-localization patterns of FT-L1 wt and FT-L1^{P95S} with Gf14s and OsFD7. *For this analysis has been used a Leica Multi-Photon Falcon Dive confocal. Co-localization pattern of FT-L1 with Gf14s is shown in A. for Gf14b and in B. for Gf14c. The localization with OsFD7 is shown in C while that of FT-L1^{P95S} with Gf14b, Gf14c and OsFD7 are in D,E and F, respectively. The green signal indicates FT-L1, whereas the orange signal indicates co-localization. Note that both FT-L1 forms co-localize with Gf14s only in the cytoplasm and with OsFD7 only in the nucleus. FT-L1 was cloned in pABind-GFP while the Gf14s and OsFD7 were cloned in pABind-mCHERRY. G. and H. indicate the subcellular localization of FT-L1-GFP and FT-L1^{P95S}-GFP, respectively.*

First, we tested the subcellular localization of FT-L1 used in these assays (fig.62G,H). FT-L1 fused with the GFP, localized both in the cytoplasm and in the nucleus.
When FT-L1, both in its WT and P95S form, was co-expressed with the Gf14s, the co-localization was observed in the cytoplasm, easily recognizable in the fig.62A,B,D,E by the merged orange channel.
When FT-L1 was co-expressed with OsFD7, the co-localization was nuclear only (fig.62C,F).

We took advantage of FLIM assays to quantify the strength of the interactions by counting the nanoseconds of GFP decay without and with the interactors (fig.63).

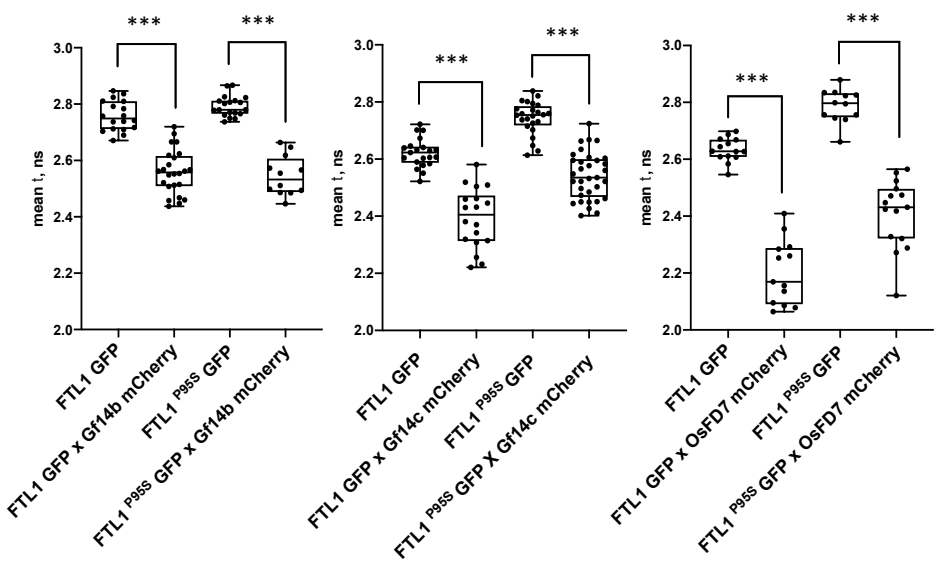

Figure 63 - Quantification of interaction strengths by FRET-FLIM measurements. *Donor lifetime was quantified in nanoseconds (ns), between FT-L1-GFP, without and with the Gf14s-mCherry and OsFD7-mCherry acceptors. Data are presented using box plots. Dots indicate measurements done on independent cells. *** P<0.0005 are based on unpaired two-tailed Student's t-test with Welch correction. All the experiments were repeated twice with identical measurements.*

As shown in the graphs in fig.63 for each interaction there is a statistically significant decrease (p value <0,0005) in the GFP lifetime indicating strong and direct interactions.

What is remarkable in this set of experiment is that no difference in interaction strength is detected between *FT-L1 WT* and *FT-L1 P95S* both with Gf14s and OsFD7.

In conclusion, we demonstrate that the mutation in position 95 is not inhibiting the binding with the Gf14s, pointing out that, for FT-L1, an intact Gf14-interaction-interface is not necessary to assemble a complex.

For the most relevant interactions detected by these two protein-protein interaction assays, some replicates are visible in fig.64A-H for BiFC assays and fig.64 I-R for FRET-FLIM experiments.

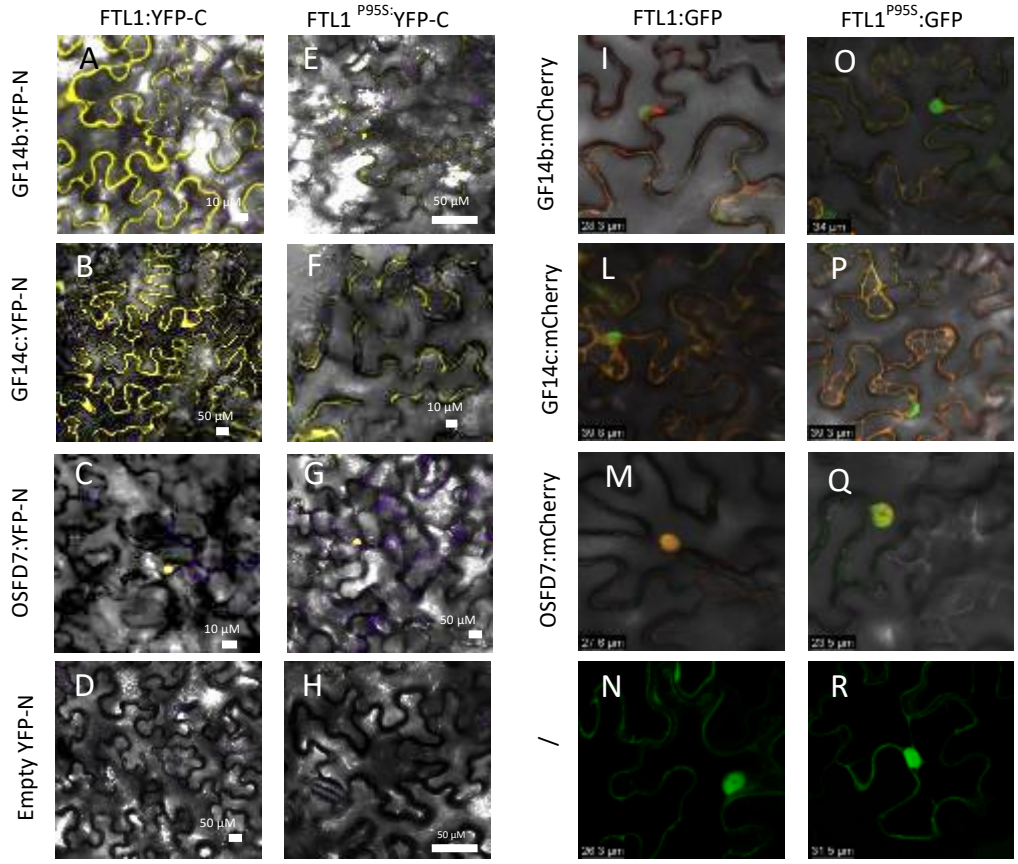

Figure 64- Additional images of protein-protein interaction analysis and co-localization patterns determined by BiFC and FLIM. *A.-H. BiFC assay. For these set of experiments, we have tested the interactions by cloning FT-L1 and FT-L1^{P95S} in pBAT TL-B sYFP-C vector (see Material and Methods section). For each interaction the localization is consistent with that detected in fig.60 and fig.61. I.-R. FRET-FLIM assay. The patterns are coherent with the ones shown in fig.62. N. and R. indicate the subcellular localization of FT-L1-GFP and FT-L1^{P95S}-GFP, respectively.*
The experiment was replicated five times with identical results.

4.7 FT-L1 – OsFD7 DIRECT INTERACTION ALLOWS TRANSITION TO SPIKELET IDENTITY

As previously described in the Introduction, OsFD7[53] is a bZIP-type transcription factor expressed in the meristem that plays a role in the definition of the panicle through the regulation of the ramifications *(see Introduction section 3.5.2- Alternative FACs)*. By directly interacting with florigens and more strongly with OsFT-L1, it carries out its function in the fine regulation of early panicle developmental (fig.65) stages and in the floral induction pathway, thus being a promoter of *SEP* family genes.

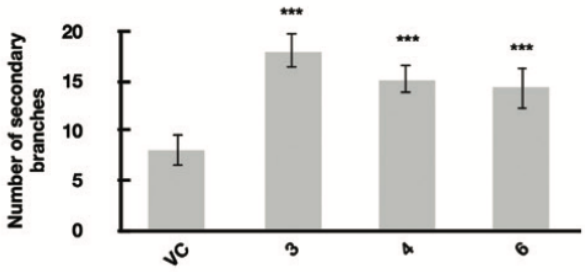

Figure 65 - Changes in panicle morphology of OsFD7 RNAi rice transgenics. *Histograms representing mean ± standard deviation of the number of secondary branches in OsFD7-RNAi transgenics lines 3,4 and 6 compared to vector control (VC) plants. ***P<0.001, Student's t-test.*[53].

Taken into consideration all this evidence, as published branching phenotype and protein-protein interaction results - also validated by our BiFC and FLIM experiments – we were pushed and intrigued to deeper investigate. In order to identify the spatial expression profile of *OsFD7*, and why it is a *FT-L1* interactor, we have performed real time PCR and *in situ* hybridization assays (fig.66A and fig.66B-D respectively).

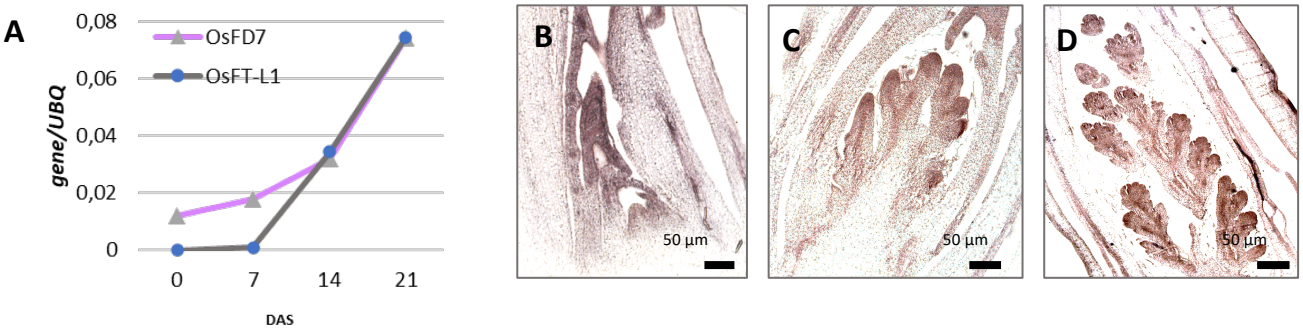

Figure 66 – Temporal and spatial expression profile of OsFD7. *A. Overlapping transcriptional dynamics of FT-L1 and OsFD7 at the SAM, upon shifting plants from LD to inductive SD. DAS, days after shift. Each time point represents mean ± standard deviation of two biological replicates each including three technical replicates. Values were normalized on the housekeeper UBQ. B-D. Expression of OsFD7 in wild type meristems determined by in situ hybridization. The signal was detected in the Vegetative Meristem (VM; B), it persisted in Primary and Secondary Branches (PBMs and SBM; C), as well as in Floret Meristem (FM; D). For this experiment only the antisense probe was used. Experiments shown were repeated five times.*

The expression analysis of meristems harvested under inductive conditions underlines the trend of expression of *OsFD7* very similar to that of *FT-L1*, with a peak of induction after 14 days after the shift into SD conditions (DAS), persisting until 21 DAS (fig.66A).

Due to its tissue localization, we have run an *insitu* hybridization (fig.66B-D) experiment to elucidate the areas of the meristematic apex where *OsFD7* gene is expressed, sampling meristems at different developmental reproductive stages.

As shown in the panel, the hybridization signal is visible in SAMs already during the vegetative stage, localizing in the vegetative and inflorescence meristems (fig.66B) then persisting during all the reproductive stages. In

the reproductive stages (fig.66C) the expression signal is localized at the terminal portions of the branches, both primary and secondary ones. In the same panel it is possible to detect also the signal in the spikelet meristems and the in the florets (fig.66D).

This expression pattern is compatible with the phenotype observed in *OsFD7* RNAi mutants[53]. These lines display an increase in secondary branch number and flower sterility, like *ft-l1* mutants, with a delay in the heading date.

In the light of these evidences, therefore, our resulting hypothesis is that FT-L1 directly interacts with OsFD7 determining the meristematic transition from SBM to SM and contributing to the determination of spikelet identity in the panicle.

4.8 FUNCTIONAL ASSAY IN *ARABIDOPSIS THALIANA*

Given what emerged from protein-protein interaction assays, such as the ability of the mutant P95S to form complexes similarly to the wt, we asked if the mutant was as functional as wt or if it is only partially functional.

To quantity its functionality, we therefore decided to conduct a complementation experiment in *Arabidopsis thaliana* (fig.67 and fig.68A,B).

To this end, we expressed both *FT-L1* forms and *FT* as positive control in the *ft-10* mutant of Arabidopsis, under the *pFD* meristem-specific promotor, obtaining *pFD: FT-L1*, *pFD: FT-L1*^{P95S} and *pFD: FT.* We selected primary transformants under non inductive SD conditions to avoid expression of TWIN SISTER OF FT (TSF) that is redundant with FT and promotes flowering under LD[104].

Figure 67 – pFD:FT-L1 complements ft-10 phenotype. *The T1 transformed plants were selected with BASTA herbicide, and flowering time was annotated by counting the rosette leaves of surviving plants. Integration of the transgenes was verified by PCR. Pictures were taken at bolting of pFD:FT-L1. At this time, plants displayed different developmental stages: pFD:FT showed advanced flowering and could complement the ft-10 phenotype, while pFD: FT-L1*^{P95S} *only partially complemented it, showing only the emergence of the inflorescence, as pointed by the red arrowhead. In the controls ft-10 and Col-0 the plants were still in the vegetative stage.*

FT and *FT-L1* misexpressors accelerated flowering time, measured as number of rosette leaves, being able to complement the *ft*-10 phenotype with a flowering time characterized by 4-10 leaves for FT and 9-20 for FT-L1. For what concerns *FT-L1*^{P95S}, instead, although partially complementing *ft*-10 phenotype, it displayed weak florigenic activity (fig. 68).

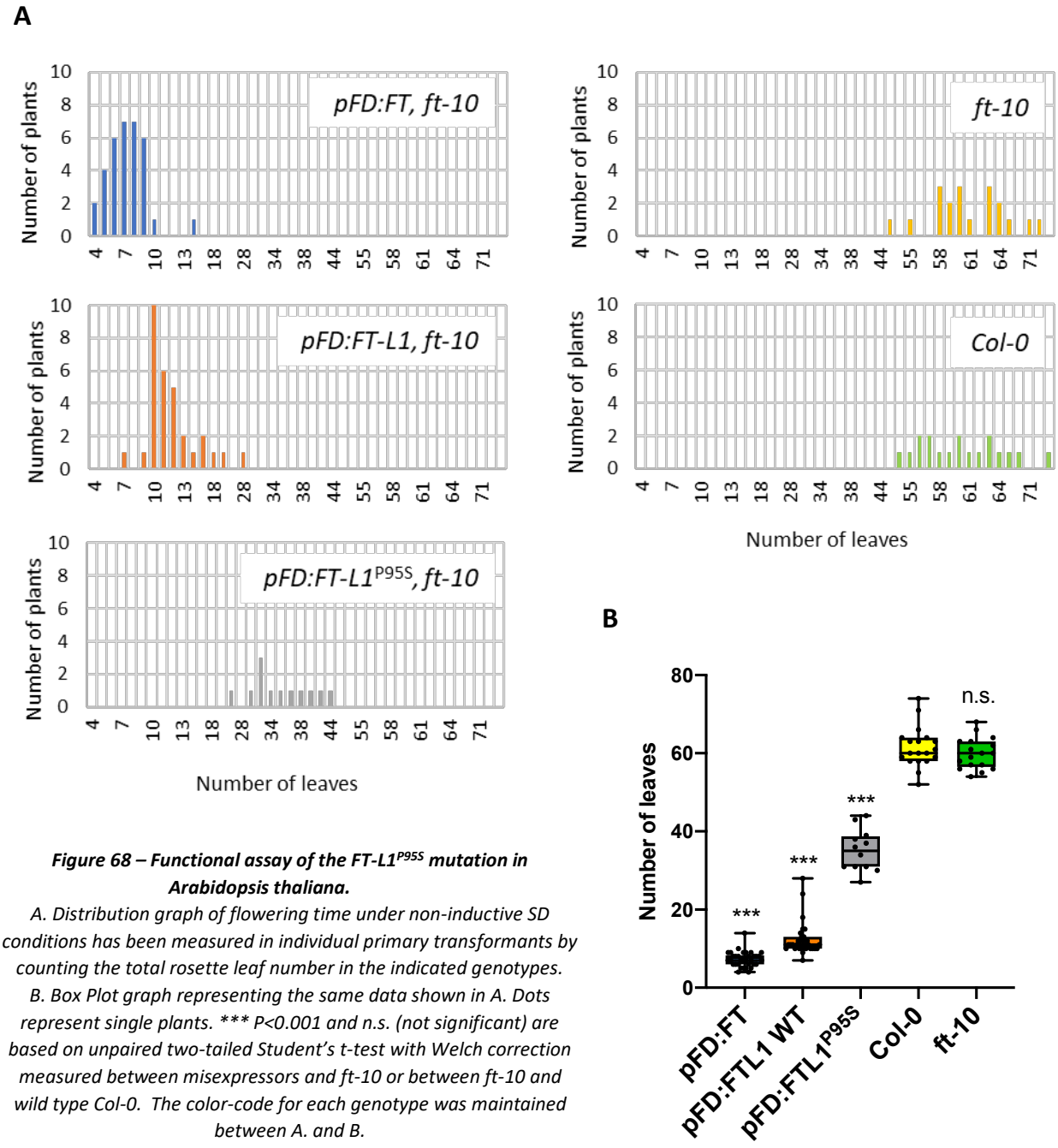

Figure 68 – Functional assay of the FT-L1^{P95S} mutation in Arabidopsis thaliana.

*A. Distribution graph of flowering time under non-inductive SD conditions has been measured in individual primary transformants by counting the total rosette leaf number in the indicated genotypes. B. Box Plot graph representing the same data shown in A. Dots represent single plants. *** P<0.001 and n.s. (not significant) are based on unpaired two-tailed Student's t-test with Welch correction measured between misexpressors and ft-10 or between ft-10 and wild type Col-0. The color-code for each genotype was maintained between A. and B.*

In conclusion we can presume that even if this mutation is actually able to assemble a FAC, it is less functional maybe due to the charge destabilization caused by the P95S substitution. Thus, this mutation is actually less functional than the WT, explaining the phenotypes observed in rice, and this might be due to its instability and/or reduced ability in activating FAC targets.